Integrative and Comparative Biology

Integrative and Comparative Biology, pp. 1–9
doi:10.1093/icb/icy094

Society for Integrative and Comparative Biology

SYMPOSIUM

A Neuromechanical Model of Larval Chemotaxis

Jane Loveless and Barbara Webb[1]

School of Informatics, University of Edinburgh, 10 Crichton Street, Edinburgh EH8 9AB, UK

From the symposium "Sensory Feedback and Animal Locomotion: Perspectives from Biology and Biorobotics" presented at the annual meeting of the Society for Integrative and Comparative Biology, January 3–7, 2018 at San Francisco, California.

[1]E-mail: B.Webb@ed.ac.uk

Synopsis Larval Drosophila move up attractive chemical gradients, and down aversive ones. Although their movement is often characterized as a series of runs and directed turns, it can also be modeled as a continuous modulation of turning extent by the detected change in stimulus intensity as the animal moves through the gradient. We show that a neuromechanical model of peristaltic crawling and spontaneous bending in the larva can be adapted to produce taxis behavior by the simple addition of a local segmental reflex to modulate transverse viscosity (or "bendiness") proportionally to the intensity change detected in the head. Altering the gain produces weaker or stronger, negative or positive taxis, with behavioral statistics that qualitatively match the larva.

Introduction

For many animals, oriented movement along sensory gradients (taxis) is an important behavior to locate key resources such as food or mates. Research into the underlying mechanisms often focuses on how taxis can be generated by the animal's nervous system, e.g., through a combination of inherent locomotion patterns for propulsion and decisions to alter direction based on sensory information. An alternative view is to consider the whole animal, embedded in its environment, as a closed loop dynamical system that can maintain a consistent output but also be biased by inputs. Importantly, in this view, the biophysical system is not just the mechanical "plant" used by the animal to execute its actions but can be a crucial part of establishing the right dynamics, by exploiting physical interactions. Similarly, this view stresses the role of the output in shaping the sensory input, potentially in just such a way as to provide the requisite input when it is needed for control.

Larval Drosophila exhibit a typical, and widely studied, taxis behavior: moving up attractive chemical gradients, and down aversive ones (Gomez-Marin et al. 2011; Gershow et al. 2012; Khurana and Siddiqi 2013; Gomez-Marin and Louis 2014). They also orient with respect to light gradients, gravity, and even electrical fields (Gepner et al. 2015); and in the absence of any clear stimulus directionality, perform exploratory behavior, with apparently spontaneous changes of direction interrupting approximately straight runs (Lahiri et al. 2011; Berni 2015). We have previously suggested that taxis could be controlled through a simple mechanism that couples the change in experienced stimulus strength directly to the amplitude of oscillation in heading direction (Wystrach et al. 2016). In the larva, this oscillation is the result of bending in the head and body segments, which alters the direction of propulsion caused by the peristaltic crawling. The larva senses odor primarily through its dorsal organ on the head (Cobb 1999), which is thus actively propelled through the gradient. In our abstracted model, we assumed the animal maintains a constant forward speed, and has a regular left/right oscillation in heading direction. The sensed change in odor concentration due to forward or lateral movement alters the subsequent oscillation amplitude. For example, an increase in concentration, indicating motion up the gradient, decreases the oscillation so the larva maintains this heading direction; whereas a concentration decrease causes it to make larger bends and hence turn back toward the source. Notably, in this control

mechanism, neither the sensing or its effect on the output is lateralized, so the "perception" of the gradient only emerges from the animal's underlying motor pattern, and subsequently shapes this pattern, in a tightly coupled feedback loop.

Although this model suggests there may be no neural correlate of "decisions to turn" in the larva, it nevertheless assumed the underlying locomotor pattern is produced by inherent control, e.g., a central pattern generator (CPG) circuit for the lateral oscillation.

More recently, we have used a biomechanical model of the larva's segmented body to explore how peristaltic crawling and lateral bending might emerge without explicit neural generation of the underlying patterns (Loveless et al. 2018). We treat the segments as discrete point masses interacting via damped translational and torsional springs, and show that using simple local reflexes to enhance the passive mechanics of the system leads to the emergence of coordinated peristaltic crawling (forward or backward) and spontaneous (chaotic) body bending. The resulting system, given frictional interaction with a substrate, produces behavior that closely resembles exploratory crawling in the larva.

In this paper, we augment this biomechanical model with a taxis reflex, following the same simple control concept as the previous abstracted model. That is, we use the change of sensory input at the head segment to influence, with a particular gain, the amplitude of the ongoing bend in each segment. The production of bends remains a purely emergent property of the mechanics without any neural control. We show that this is sufficient to produce positive or negative taxis in the simulated agent, depending on the sign of the gain, and stronger or weaker taxis depending on the size of the gain. We discuss similarities and differences from taxis behavior in real larva.

Methods

Neuromechanical model

The work presented here builds on an existing model of larval crawling, described in detail in Loveless et al. (2018). We here provide an overview of the model, but refer readers to that paper for detailed specification (see Online Appendix S1), justification, and analysis. The model describes the motion of the midline of the larval body in the plane using 12 points that represent the boundaries between body segments and the head and tail extremities. Each point is treated as an identical mass, and each is linked to adjacent points with linear translational and torsional springs in parallel with linear dampers in a Kelvin–Voigt arrangement (Fung 1993), to represent elasticity in the soft cuticle of the larva (Fig. 1). The current body configuration can thus be expressed as a set of axial stretches q_i (the difference in length of the ith segment from its length at equilibrium) and transverse bending angles between segments φ_i. The head and tail are additionally linked, representing the effect of the incompressible internal coelemic fluid of the larva, by maintaining a constant overall length. Without friction, the passive mechanics of this system produces axial and transverse standing waves, i.e., coordinated motions of the segments that resemble peristalsis and body bends.

We assume there is sliding friction between the larval body and the substrate, and energy is also lost to viscous friction within the body during both axial compression/extension and transverse bending. We allow power flow due to muscle activation, controlled by two reflexes (Fig. 1). The first is local to each segment and acts to overcome the effects of friction, by activating whenever a segment is compressing, producing a muscle tension that amplifies the compression. The axial tension Q_i in the ith segment produced by this reflex is given in terms of the local stretch rate $\dot{q}_i$ and local axial reflex gain b_i as

$$Q_i = \begin{cases} -b_i, & \text{if } \dot{q}_i < 0 \\ 0, & \text{if } \dot{q}_i \geq 0 \end{cases}. \quad (1)$$

The second neural circuit is a mutual inhibition between non-adjacent segments (the head and tail are treated as adjacent) that restricts the active compression to a small number of segments at any time. This enables acceleration of the center of mass relative to the substrate, i.e., peristaltic crawling (Alexander 2003; Ross et al. 2015; Loveless et al. 2018). Due to energetic coupling of axial and transverse motion, through the body mechanics, the model also produces spontaneous body bending, which reorients the crawling direction, i.e., turning occurs without any explicit neural control.

This emergent turning produces a "random" (actually a deterministically chaotic) exploration of the 2D plane. To convert the resulting exploration into taxis, we note that the larva should travel in a roughly straight line while going up an attractive gradient, or while going down an aversive gradient, and that the larva should tend to reorient when it is going down an attractive gradient, or going up an aversive gradient. In other words, the extent of the body bending should be linked to the changing perceptual experience (Fig. 2). We can affect bending by altering the effective physics of the body: specifically, we reason that an effective increase in transverse viscosity should lead to a damping of transverse motion

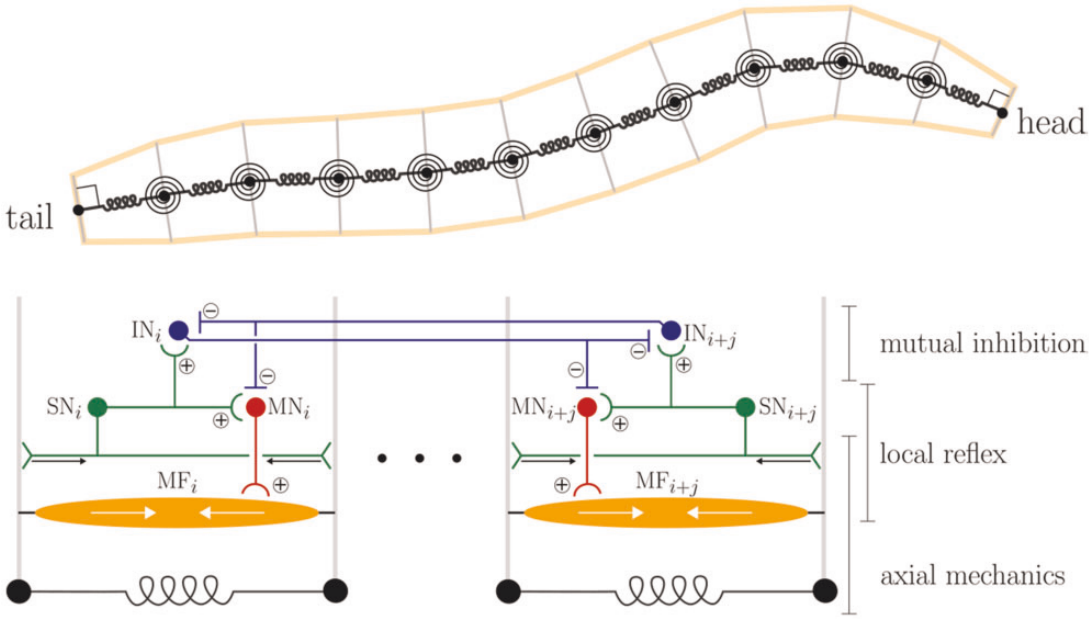

Fig. 1 The larva is represented by a mechanical model (top) of its midline with 11 segments. The boundaries between segments are treated as point masses linked by linear translational and torsional springs in parallel with linear dampers in a Kelvin–Voigt arrangement (Fung 1993). The controller (bottom) uses positive feedback within each segment to counteract friction and distant inhibition between non-adjacent segments to create a coherent peristaltic wave of contraction capable of driving locomotion. The mechanics produce spontaneous body bending without any explicit neural control.

Source: From Loveless et al. (2018).

and a corresponding tendency toward straight line motion, while an effective decrease in transverse viscosity should reduce the damping of transverse motion and therefore tend to encourage bending and reorientation. We thus posit the following local segmental reflex for transverse motion:

$$\tau_i = c_i \tanh(\beta \dot{\phi}_i) \tanh(\gamma P(t)), \tag{2}$$

where τ_i is the torque applied about the ith segment boundary, $P(t)$ is the time-varying perception input (defined below), β is an angular velocity gain, γ is a perception gain, and c_i is an overall reflex gain for the ith segment boundary. We limit the choice of parameters by setting $\beta > 0$ and $c_i > 0$, so that the sign of the torque is determined by γ.

The rationale of our reflex model can be understood by splitting it into two factors. The first factor $c_i \tanh\left(\beta \dot{\phi}_i\right)$ represents (saturating) feedback of the local angular velocity. The torque resulting from this first factor only should act in the same direction as the angular velocity, opposing the torque produced by transverse friction, and thereby reducing the effective transverse viscosity of the body (i.e., preventing the "bendiness" of each segment being limited by friction). Following this line of reasoning, we choose to set the local reflex gain c_i to be dependent upon the local transverse viscosity $\eta_{t,i}$

$$c_i = c \frac{\eta_{t,i}}{\max_i \eta_{t,i}}, \tag{3}$$

where normalization by $\max_i \eta_{t,i}$ is intended to nondimensionalize the transverse viscosity, allowing the new global reflex gain parameter c to have dimensions of torque. In practise we set $c = 1$ for simplicity, leaving

$$c_i = \frac{\eta_{t,i}}{\max_i \eta_{t,i}} \tag{4}$$

so that the reflex torque becomes

$$\tau_i = \frac{\eta_{t,i}}{\max_i \eta_{t,i}} \tanh(\beta \dot{\phi}_i) \tanh(\gamma P(t)). \tag{5}$$

The second factor $\tanh(\gamma P(t))$ acts to modulate the change in effective transverse friction based on perception. If this factor is positive, the overall effect of the reflex is to reduce effective transverse viscosity, while if it is negative the effect is reversed and effective transverse viscosity increases. If the overall feedback torque is small (e.g., if β, γ, or c are relatively close to zero) then the perception input will have a small effect on the transverse viscosity, while if the overall feedback torque is large there is the possibility for the perception input to have a large effect on the transverse viscosity. This provides an interpretation of the perception gain γ as a preference parameter—if the absolute value of γ is large, the model larva

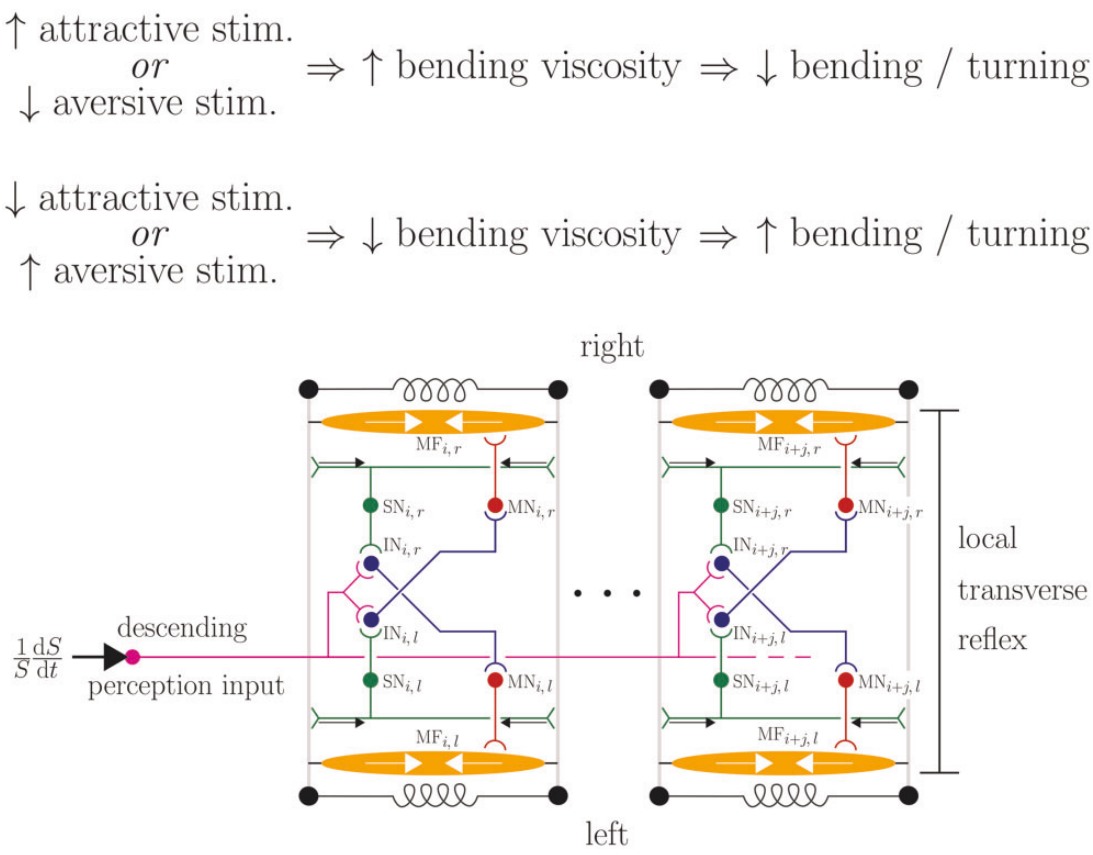

Fig. 2 Taxis is achieved by increasing (decreasing) transverse viscosity during favorable (unfavorable) stimulus conditions, thus leading to decreased (increased) bend/turn amplitude (top panel). This could be achieved through descending chemosensory innervation of a segmentally localized contralateral reflex acting to modulate the effective local transverse viscosity (bottom panel, see text).

should show a strong behavioral response to the stimulus, while for small γ the behavioral response may be weak. Furthermore, following our arguments above, if $\gamma>0$ we expect an aversive response, while for $\gamma<0$ we expect an attractive response. We note a further expectation that the strength of the behavioral response when $\gamma>>1$ may be diminished due to saturation of the second factor in Equation (2) and a corresponding inability to distinguish small changes in perception—in this case, the second factor can only detect whether the head is traveling up or down gradient, but not how strong the local gradient is. Note that the effectiveness of this proposed functional relation between torque and perception for producing taxis results largely from the qualitative properties just discussed, rather than being strongly dependent upon the precise formulation given. As such, Equation (5) represents a simple and interpretable way to implement the desired relationship.

Perceptual model

We model the larva as moving within an exponential stimulus field centered on the origin of our Cartesian coordinate frame

$$S = A_s e^{-\lambda_s ||\mathbf{r}||}, \tag{6}$$

where A_s is a parameter which sets the absolute intensity of the stimulus field, and λ_s sets the rate at which the stimulus decays away from the origin, while $\mathbf{r}$ is the radius vector from the origin to the site of measurement of the stimulus. In practice, we take $\mathbf{r}$ to be the radius vector from the stimulus source to the model larva's head, since this is the location of most of the sensory organs involved in taxis.

The early stages of sensory processing in the larva tend to respond strongly to changes in stimulus intensity more than to the absolute stimulus intensity, and show a normalized response across a range of absolute stimulus intensities. Following Davies et al. (2015), we model the output of the early stages of sensory processing as a "perception" signal given by

$$P = \frac{1}{S}\frac{dS}{dt}. \tag{7}$$

Denoting the coordinates of the larva's head as $\mathbf{r} = [x, y]^T$ and the linear velocity of the larva's head as $\dot{\mathbf{r}} = [\dot{x}, \dot{y}]$, this becomes

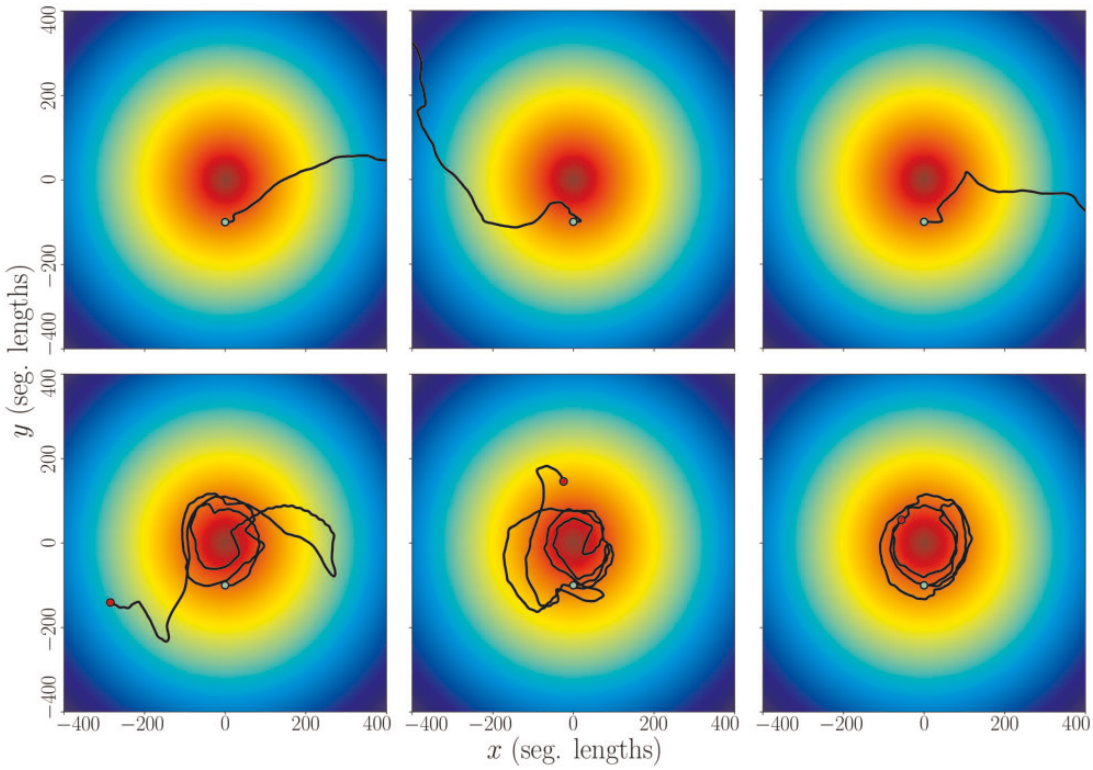

Fig. 3 Changing the perception gain/preference parameter γ causes the model larvae to exhibit increasingly attraction. Representative trajectories are shown for $\gamma = 1000$, 200, 100 (aversive behavior, top row, left-to-right) and $\gamma = -100$, -200, -1000 (attractive behavior, bottom row, left-to-right). Trajectories start at the light/green circle, end at the dark/red circle (larvae doing negative taxis escaped the area shown), and are superimposed on a map of the log stimulus intensity.

$$P = \frac{1}{S}\left(\frac{\partial S}{\partial x}\dot{x} + \frac{\partial S}{\partial y}\dot{y}\right) = \frac{1}{S}\nabla S \cdot \dot{\mathbf{r}} \tag{8}$$

substituting the expression for the exponential stimulus field given above, we find

$$\nabla S = -\frac{A_s \lambda_s}{\sqrt{x^2 + y^2}}[x, y]^T \tag{9}$$

so that

$$P = -\lambda_s \frac{x\dot{x} + y\dot{y}}{\sqrt{x^2 + y^2}} = -\lambda_s \frac{\mathbf{r} \cdot \dot{\mathbf{r}}}{||\mathbf{r}||} = \lambda_s ||\dot{\mathbf{r}}|| \cos\theta, \tag{10}$$

where θ is the angle between the head's velocity vector $\dot{\mathbf{r}}$ and the vector pointing from the head position to the origin $-\mathbf{r}$. As expected, P is positive when the larva is traveling up the sensory gradient ($|\theta| < \pi/2$), negative when the larva is traveling down the sensory gradient ($|\theta| > \pi/2$), and has a magnitude which depends on both the speed at which the head is traveling and on the bearing of the head to the odor source. Note that due to normalization of the sensory input, the absolute intensity parameter A_s has no effect on the perception signal.

Substituting this definition of P into to the transverse reflex Equation (2), we have

$$\tau_i = \frac{\eta_{t,i}}{\max_i \eta_{t,i}} \tanh(\beta\dot{\phi}_i)\tanh(\gamma\lambda_s||\dot{\mathbf{r}}||\cos\theta), \tag{11}$$

which makes it clear that there is some redundancy in the parameters γ and λ_s, so that we may set $\lambda_s = 1$ without loss of generality. This leaves two free parameters in the transverse reflex model, β and γ. We choose to set $\beta = 1000 \gg 1$ so that the factor $\tanh\left(\beta\dot{\phi}_i\right)$ saturates to ± 1, matching our binary-valued axial reflex (Equation 1). This leaves us to explore possible values of the perception gain/preference parameter γ.

We set all mechanical parameters and the parameters for the axial reflex circuits to the values chosen in our previous paper (Loveless et al. 2018), with the exception of the transverse viscosity $\eta_{t,i}$ which has been set to twice its previous value. This choice was made in order to more clearly demonstrate the action of the transverse reflex on the model behavior.

Results

In Fig. 3, we show some representative trajectories generated by our taxis model (see also Supplementary Videos). In each case the larva starts at the peak of the gradient. For positive gains it crawls away, eventually exiting the space. For

negative gains, it consistently loops back toward the peak, with the extent of excursions decreasing as the strength of the gain is increased. The tendency to orbit rather than approach or dwell at the exact peak of the gradient was also observed in our previous model and in larvae (Wystrach et al. 2016).

To analyze the behavior of our taxis model, we generated $N = 1000$ trajectories for each of the cases $\gamma = \pm 200$. As expected the larvae with $\gamma = -200$ showed a strong approach behavior, remaining localized near the peak of the stimulus field (Fig. 4A), while larvae with $\gamma = 200$ showed strong avoidance behavior, following fairly direct paths away from the peak (Fig. 4B) (note at the periphery, larvae will have exited the defined area of the gradient).

We first quantified the paths of the simulated larvae using the same methods we applied to the unbiased exploratory paths presented in our previous paper (Loveless et al. 2018). Paths in the approach group ($\gamma = -200$) had a high tortuosity and fractal dimension (mean tortuosity = 0.72, mean fractal dimension=1.51) relative to the avoidance group ($\gamma = 200$, mean tortuosity = 0.11, mean fractal dimension = 1.22; Fig. 4C), indicating that approach paths tended to be plane-filling and less linear than avoidance paths (Benhamou 2004). In accordance with these results, the mean-squared displacement measured within the avoidance group followed an approximately quadratic growth across the duration of the entire experimental trial, typical of rectilinear motion, whereas the approach group showed an initial quadratic growth followed by linear and then sub-linear growth (Fig. 4D). We previously found that our model of unbiased exploration produced initially quadratic growth of the mean-squared displacement, followed by asymptotic linear growth (Loveless et al. 2018), as has also been observed during unbiased exploration in the real larva (Jakubowski et al. 2012; Gunther et al. 2016). This suggests that our modeled taxis reflex can be interpreted, at the population level, as biasing an ongoing deterministic anomalous diffusion process into either superdiffusive ($\gamma > 0$, quadratic growth) or subdiffusive ($\gamma < 0$, sub-linear growth) regimes.

The distribution of body bending angles (Fig. 4E) shows that the modeled larvae take on "straighter" configurations during avoidance behavior (mean $= 4.6 \times 10^{-3}$ deg, variance = 75.5 deg^2, kurtosis = 13.17), and tend to take on larger curvatures during approach behavior (mean = 0.11 deg, variance = 853.52 deg^2, kurtosis = 1.94), in accordance with the rationale for our taxis reflex model and in agreement with the shape of paths taken by the two groups. During both avoidance and approach, the body bend distribution is symmetric (avoidance skewness = 0.02, approach skewness = 0.07) and centered around 0 (avoidance mean $= 4.6 \times 10^{-3}$ deg, approach mean = 0.11 deg), demonstrating that the model larvae are not, on aggregate, biased toward bending either to the left or the right. The "shoulders" observed in the distribution of bends for approach reflect physical constraints of larger bends in the mechanical model.

Although the body bend distribution is continuous in our model, it is convenient for comparison to real larvae to divide motion across the substrate into "runs" and "turns," by classifying a turn as a body bend of >20°. The run length distribution of both avoidance and approach groups is well fit by an exponential, but avoidance behavior is biased toward longer runs when compared with approach behavior (avoidance time constant = 44.49 s, approach time constant = 10.67 s; Fig. 4F), as is also seen in the real larva during thermotaxis (Luo et al. 2010).

We also analyzed the behavior of our model using three measures which are common in the extant literature on taxis behavior. These measures depend upon the bearing angle between our larva's centre of mass velocity and the local gradient of the stimulus field.

First, we examined the overall distribution of bearing angles for our simulated larvae (Fig. 4G). Similar to results for the real larva (Wystrach et al. 2016), the bearing distribution for avoidance behavior was unimodal, symmetric, and centered on 180°, and fell to zero outside of the range [90°, 270°], corresponding to travel directly away from the stimulus peak. In contrast, the bearing distribution for approach behavior was trimodal, with a pair of large, symmetric peaks centered falling below 90° and above 270° and a single shallow peak at 180°. This corresponds to a large amount of time spent "spiralling" toward the stimulus peak, with the peak located mostly to the left or right of the animal.

Next, we computed the probability density of turns (defined to occur at the onset of a body bend >20°) across absolute bearing angle (Fig. 4H). Both approach and avoidance behaviors showed a monotonic increase in turn probability as absolute bearing increased from 0° (bearing toward stimulus peak) to 180° (bearing away from stimulus peak). Similar to the real larva (Davies et al. 2015), the turn probability for approach behavior in our model showed a roughly sigmoid shape, with greater probability assigned to intermediate bearings (~90°) and less to large bearings (~180°) than during avoidance behavior, which followed a roughly exponential distribution.

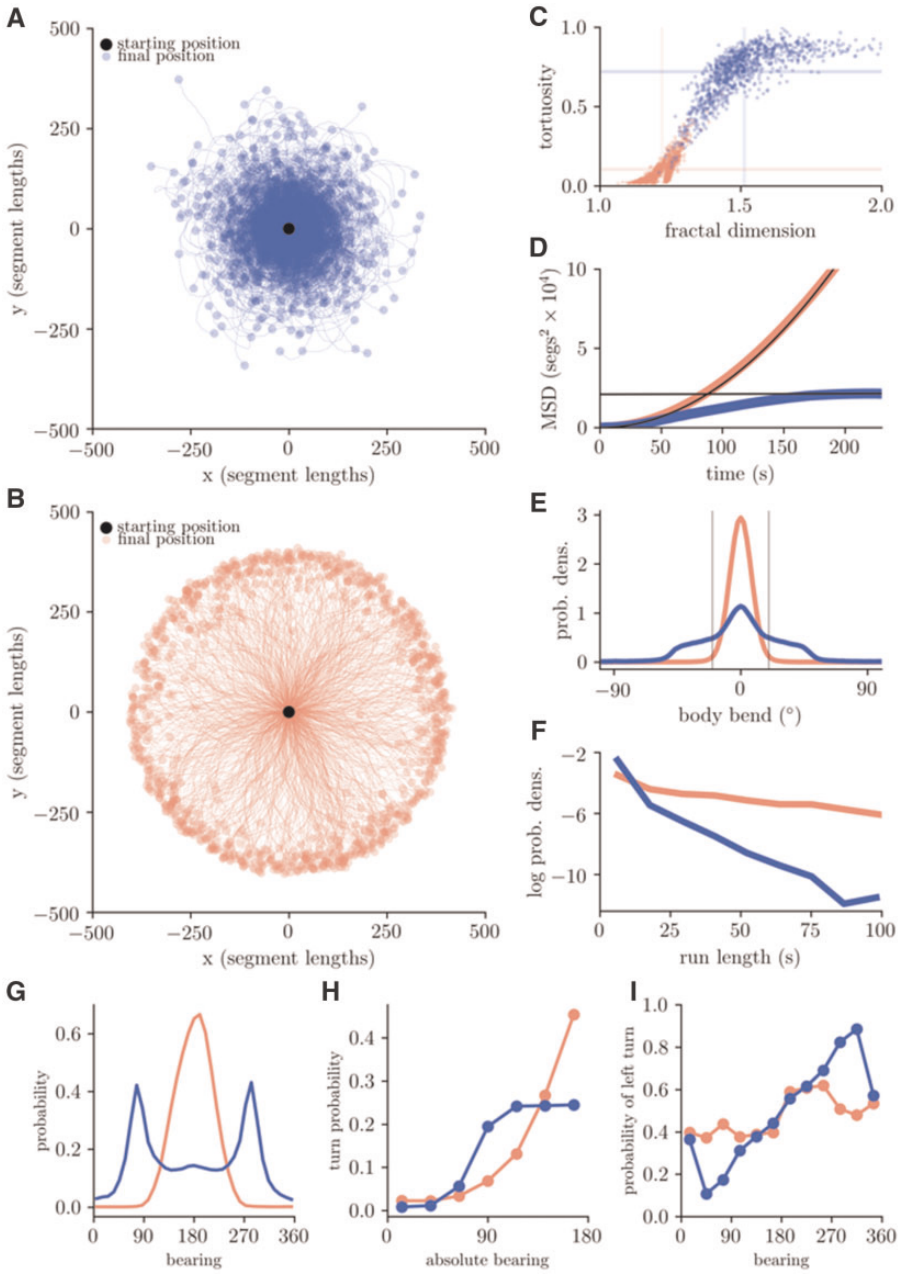

Fig. 4 Analysis of positive ($\gamma = -200$) and negative ($\gamma = 200$) taxis behavior in $N = 1000$ simulated larvae. **A**: center of mass trajectories for the simulated larvae during positive taxis. **B**: trajectories during negative taxis. Larvae started from almost identical configurations but with random orientation. **C**: larval paths show higher tortuosity and fractal dimension during positive taxis (blue/dark) compared with negative taxis (red/light; horizontal lines = mean tortuosity, vertical lines = mean dimension), indicating rectilinear motion during negative taxis and plane-filling motion during positive taxis. **D**: mean-squared displacement shows asymptotic quadratic growth during negative taxis and absence of growth during positive taxis. **E**: distribution of body bends. **F**: distribution of run durations during negative and positive taxis. Run lengths were calculated as duration between successive crossings of a threshold body bend (20°), indicated by vertical lines in panel **E**. **G**: probability distribution of bearings to stimulus source. **H**: turn probability as a function of absolute bearing angle. **I**: probability of left turn as function of bearing angle.

Finally, we measured the probability of the larva turning to the left rather than right side, across bearing angles (Fig. 4I). The model larvae exhibiting approach behavior showed a strong bias for turning toward the stimulus peak (probability of left turn <0.5 for bearing$\in[0°, 180°]$, probability of left turn >0.5 for bearing $\in[180°, 360°]$), which is similar to results for the real larva (Davies et al. 2015). Model larvae exhibiting avoidance behavior showed a much weaker bias, though perhaps surprisingly, in

the same direction. For real larvae this curve appears flat for aversive behavior.

Discussion

Behavior emerges from the coupling of brains and bodies. We have combined a model of segmented larval biomechanics with a simple, non-lateralized reflex and shown this can produce directed taxis up or down a sensory gradient. The key mechanism is to modulate spontaneous mechanically-driven bending by adjusting transverse viscosity in each segment proportionally to the immediately perceived change in stimulus intensity. By altering the gain factor, the behavior produced can be stronger or weaker attraction (with negative gain) or stronger or weaker aversion (with positive gain). That is, if an increase in the sensory signal is coupled to a damping of transverse motion, the larva will tend to go straight when going up a gradient and reorient more when going down it, ultimately leading it toward the sensory source, and vice versa for the opposite signal-damping coupling.

We note that, for the values of negative gain examined here, this mechanism tends to produce "orbiting" behavior with the sensory source predominantly at around 90 degrees to the larva, while for positive gain larvae display dispersive behavior with the source remaining behind the larva. Similar distributions of bearing angles are observed for real larva (Wystrach et al. 2016). Indeed, our model also qualitatively reproduces the distribution of run durations observed during approach and avoidance (Luo et al. 2010), as well as the experimentally observed distributions of turn probability and left-turn probability over bearing angle (Davies et al. 2015).

Several of these characteristics have been captured in previous models of larval chemotaxis. In Davies et al. (2015), the probability of transition from a "run" to a "turn" was altered by the change in odor intensity, and a similar approach was coupled to a more realistic model of olfactory sensory neuron responses in Schulze et al. (2015). In Wystrach et al. (2016) it was proposed that the distinction between runs and turns be replaced by a continuum of smaller or larger oscillations in heading direction, and shown that this could replicate many aspects of the behavior without requiring "decisions" to turn. The current model is in the spirit of this latter approach, but dispenses with any need to posit an underlying CPG to generate body bends, as these emerge spontaneously from the inherent dynamics of forward crawling in coupled segments (Loveless et al. 2018). As such, if "turns" are identified with larger bends, then their chaotic generation can replace the probabilistic approach of the earlier models and the distinction between these explanations becomes less marked. More generally, we acknowledge that the precise form of the relationship between bend amplitude and perception presented here is not crucial to obtain taxis. Rather, we have shown that it is straightforward to extend our mechanical model of crawling to taxis, and this does not require the perceptually-driven turning signal to be lateralized or differentiated between segments.

Although the presented model uses direct control of torque to counter or reinforce the effects of transverse viscosity, a biologically plausible means to achieve this effect would be a neural reflex circuit that couples the muscles on one side of a body segment to proprioceptive sensory neurons on the opposite side (see Fig. 4). The effective transverse viscosity will be increased if muscles on one side of the body contract while the opposite side is shortening, while the effective viscosity will be decreased if muscles contract while the opposite side is lengthening. The EL neurons reported in (Heckscher et al. 2015) appear to be a possible substrate for this function. We then need only add a general signal (to all segments) that modulates the action of this local reflex. Neurons that run throughout the ventral nerve cord and connect the brain to all segments have been identified (Fushiki et al. 2016). It is also of interest that a small set of neurons in the brain's premotor subesophgeal zone appear to directly affect the production of large reorientations (high head angular speeds) in larva, with the same effects observed for taxis in odor, light, and temperature gradients (Tastekin et al. 2015). Finally, we note that the action of the local reflex could be enhanced by the presence of reciprocal inhibition, acting to relax the muscles on one side of the body while those on the other side contract—such inhibitory pathways are a common feature in the spinal reflexes of jointed animals, including humans (Purves et al. 2004).

Funding

This research was supported by the FP7 Framework FET-Open grant "MINIMAL."

Supplementary data

Supplementary data available at *ICB* online.

References

Alexander RM. 2003. Principles of animal locomotion. 1st ed. Princeton (NJ): Princeton University Press (ISBN 9781400849512).

Benhamou S. 2004. How to reliably estimate the tortuosity of an animal's path: straightness, sinuousity, or fractal dimension? J Theor Biol 229:209–20.

Berni J. 2015. Genetic dissection of a regionally differentiated network for exploratory behavior in *Drosophila* larvae. Curr Biol 25:1319–26.

Cobb M. 1999. What and how do maggots smell? Biol Rev 74:425–59.

Davies A, Louis M, Webb B. 2015. A model of *Drosophila* larva chemotaxis. PLoS Comput Biol 11:e1004606–24.

Fung Y-C. 1993. Biomechanics: mechanical properties of living tissues. 2nd ed. New York (NY): Springer-Verlag (ISBN 978-0-387-97947-2).

Fushiki A, Zwart MF, Kohsaka H, Fetter RD, Cardona A, Nose A. 2016. A circuit mechanism for the propagation of waves of muscle contraction in *Drosophila*. eLife 5:e13253.

Gepner R, Mihovilovic Skanata M, Bernat NM, Kaplow M, Gershow M. 2015. Computations underlying *Drosophila* photo-taxis, odor-taxis, and multi-sensory integration. eLife 4:e06229 (ISSN 2050-084X).

Gershow M, Berck M, Mathew D, Luo L, Kane EA, Carlson JR, Samuel ADT. 2012. Controlling airborne cues to study small animal navigation. Nat Methods 9:290–6.

Gomez-Marin A, Louis M. 2014. Multilevel control of run orientation in *Drosophila* larval chemotaxis. Front Behav Neurosci 8:1–14.

Gomez-Marin A, Stephens GJ, Louis M. 2011. Active sampling and decision making in *Drosophila* chemotaxis. Nat Commun 2:1–10.

Gunther MN, Guilherme N, Shubeita GT. 2016. Quantifying and predicting *Drosophila* larvae crawling phenotypes. Sci Rep 6:1–10.

Heckscher ES, Arzan Zarin A, Faumont S, Clark MQ, Manning L, Fushiki A, Schneider-Mizell CM, Fetter RD, Truman JW, Zwart MF, et al. 2015. Even-skipped^{+} interneurons are core components of a sensorimotor circuit that maintains left–right symmetric muscle contraction amplitude. Neuron 88:314–29.

Jakubowski BR, Longoria RA, Shubeita GT. 2012. A high throughput and sensitive method correlates neuronal disorder genotypes to *Drosophila* larvae crawling phenotypes. Fly 6:303–8.

Khurana S, Siddiqi O. 2013. Olfactory responses of drosophila larvae. Chem Senses 38:315–23.

Lahiri S, Shen K, Klein M, Tang A, Kane E, Gershow M, Garrity P, Samuel ADT. 2011. Two alternating motor programs drive navigation in *Drosophila* larva. PLoS One 6:e23180 (ISSN 1932-6203).

Loveless J, Lagogiannis K, Webb B. 2018. Modelling the mechanics of exploration in larval *Drosophila*. PLoS Comput Biol (https://www.biorxiv.org/content/early/2018/07/03/354795).

Luo L, Gershow M, Rosenzweig M, Kang KJ, Fang-Yen C, Garrity PA. 2010. Navigational decision making in *Drosophila* thermotaxis. J Neurosci 30:4261–72.

Purves D, Augustine GJ, Fitzpatrick D, Hall WC, LaMantia A-S, McNamara JO, Williams SM. (eds.). 2004. Neuroscience. 3rd ed. Sinauer Associates, Inc.

Ross D, Lagogiannis K, Webb B. 2015. A model of larval biomechanics reveals exploitable passive properties for efficient locomotion. Proceedings of Conference on Biomimetic and Biohybrid Systems, Barcelona July 2015. Springer International Publishing. p. 1–12.

Schulze A, Gomez-Marin A, Rajendran VG, Lott G, Musy M, Ahammad P, Deogade A, Sharpe J, Riedl J, Jarriault D, et al. 2015. Dynamical feature extraction at the sensory periphery guides chemotaxis. eLife 4:e06694 (ISSN 2050-084X).

Tastekin I, Riedl J, Schilling-Kurz V, Gomez-Marin A, Truman JW, Louis M. 2015. Role of the subesophageal zone in sensorimotor control of orientation in drosophila larva. Curr Biol 25:1448–60.

Wystrach A, Lagogiannis K, Webb B. 2016. Continuous lateral oscillations as a core mechanism for taxis in *Drosophila* larvae. eLife 5:e15504.